PCCP

Accepted Manuscript

ROYAL SOCIETY OF CHEMISTRY

www.rsc.org/pccp

Nitrogen doping can greatly increase O_w activity, which affect the mercury oxidation /chemical adsorption abilities on $CuCo_2O_4(110)$ surface.

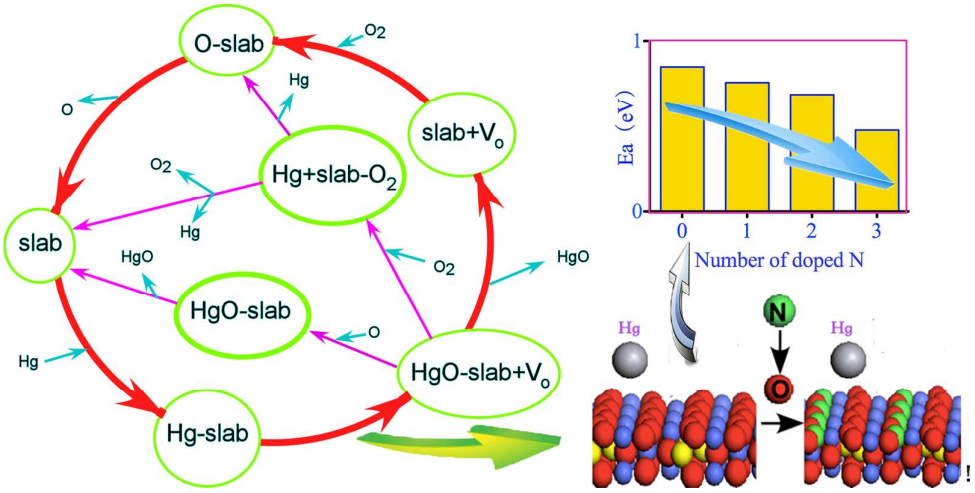

Cite this: DOI: 10.1039/c0xx00000x

www.rsc.org/xxxxxx

ARTICLE TYPE

Effect of nitrogen doping on the mercury oxidation/chemical adsorption on $CuCo_2O_4$ (110) surface: a molecular-level description

Zhijian Mei,*[a] Maohong Fan,[b,c] Ruiqing Zhang,[a] Zhemin Shen[d] and Wenhua Wang[d]

Received (in XXX, XXX) Xth XXXXXXXXX 20XX, Accepted Xth XXXXXXXXX 20XX

DOI: 10.1039/b000000x

Based on density functional theory (DFT) calculations, the detailed mercury oxidation/chemical adsorption mechanisms on the N-doped $CuCo_2O_4$(110) surface are studied. The DFT calculations show that O_w (bonded with one Cu^{2+} ion and one Co^{3+} ion) is far more active than O_s (bonded with three Co^{3+} ions) and the mercury oxidation/chemical adsorption activation energy (E_a) on virgin $CuCo_2O_4$(110) surface involving O_w is 0.85 eV. The physical adsorbed mercury overcomes the E_a and enters energy well that plays an important role in the mercury oxidation/chemical adsorption. Nitrogen doping can greatly increase the activity of O_w and decrease the activity of O_s at the same time, which greatly affect the mercury oxidation/chemical adsorption abilities on $CuCo_2O_4$(110) surface and the E_a variation of the mercury oxidation/chemical adsorption are as follows: 0.85 eV (virgin $CuCo_2O_4$(110)) → 0.76 eV (one N-doped $CuCo_2O_4$(110)) → 0.69 eV (two N-doped $CuCo_2O_4$(110)) → 0.48 eV (three N-doped $CuCo_2O_4$(110)). In addition, N-doping can decrease the adsorption energy of mercury and mercuric oxide. The effect of N-doping on the bonding mechanism of mercury adsorption on $CuCo_2O_4$(110) surface is analyzed by local density of state (LDOS) and natural bonding orbit (NBO). The calculation results are corresponding well to the experimental data.

1. Introduction

Complex oxides (containing two or more types of cations) with spinel structure are of intense interests in material research because of their remarkable optical, electrical, magnetic, catalytic properties and widespread applications in science and engineering[1]. Among these, spinel cobaltites (MCo_2O_4; M: Co, Cu, Mn, Ni, Zn, Mg, etc.) have recently drawn considerable attention by virtue of their superior physicochemical properties and tremendous potential for many technological applications, ranging from catalysts and sensors to electrode materials and electrochromic devices [2].

Copper cobaltite with the general formula $Cu_xCo_{3-x}O_4$ is well known for the catalytic activity towards the oxidation of CO to CO_2, carbon monoxide hydrogenation, mercury oxidation, anode for lithium-ion batteries, automobile pollution control and oxygen evolution[3-10]. Copper cobaltite spinel crystals with various structural/morphological characteristics (i.e., particle size, shape, stoichiometry and cation distribution) can be prepared by diverse synthetic routes including nitrate decomposition[4], urea combustion[11], co-precipitation[12], sol–gel[13], hydrothermal[14], aerosolpyrolysis [15], anodic electrodeposition [16] and so forth.

The nonmetal doping technique has been investigated as an alternative approach to the photocatalytic degradation of various environmental pollutants and the interstitial nonmetal atoms are responsible for visible-light response[17]. Halide ions, such as Cl^- and F^-, are used to decrease lattice oxygen activity and enhance the redox strength of perovskite-type oxides (ABO_3). The halogen-doped process can convert these materials to selective catalysts for the oxidation of ethane to ethene[18, 19]. Usually, the cation Cu^{2+} in spinel $CuCo_2O_4$ is used to replace the Co^{2+} in $CoCo_2O_4$ to modify its catalytic activity. Except for the cation, the anion O in $CoCo_2O_4$ or $CuCo_2O_4$ can be replaced by other nonmetal elements to modify their catalytic activity. In previous work, nitrogen-doping is used to improve the Hg^o oxidation/chemical adsorption ability of $CuCo_2O_4$[20]. However, the associated reaction mechanisms are not clear and need to be further explored[21]. This is because the reaction mechanisms can help us understand how the doped nonmetals affect the activity of $CuCo_2O_4$. Specifically, it is of great interest to know the location of the doped nonmetals, to predict the properties of the materials doped with other nonmetals, and to understand the mechanisms involved, which can help building a new atlas for the design of cost-effective materials.

To study the mercury oxidation/chemical adsorption mechanism on different nitrogen doped $CuCo_2O_4$, the density functional theory (DFT) that has been widely used to research the mechanisms of reactions on the surface of transition metals and metal oxides is needed[22-25]. In the present word, a periodic self-consistent DFT investigation in mercury oxidation/chemical adsorption on the surfaces of virgin $CuCo_2O_4$(110) and other different N-doped $CuCo_2O_4$(110) is performed, and the thermochemistry and detailed energetic aspects of the elementary steps are discussed.

2. Methods

The calculations of the total energy associated with the Hg adsorption on the surface of $CuCo_2O_4$(110) are carried out using the CASTEP in Materials Studio software package. Ultrasoft pseudopotential (USP) is chosen as the parameter in all calculations. The generalized gradient approximation (GGA) proposed by Perdew et al. (Perdew–Burke–Ernzerh, PBE) is employed to estimate the exchange-correlation potential[26]. Because the N-doped system that bring problems for the U and J determination and our concerns, DFT+U is not used. In this

study, the clean surfaces of four-layer p(2×2)-$CuCo_2O_4$(110) slab separated by a vacuum of 20 Å are modeled[27]. The cut-off energy of plane-wave is 380 eV. 4×4×1 k-point grid for the p(2×2) cell with Monkhorst-Pack scheme is used because preliminary calculations indicated that energy is sufficiently convergent. During our calculations, the positions of two top layers of $CuCo_2O_4$(110) slab and Hg molecules are assumed to be mobile with the forces on the ions being less than 0.02 eV/Å while the positions of two bottom layers are fixed. Furthermore, a 0.1 eV Fermi broadening band is chosen to smear the occupation of the bands around E_F using a finite-*T* Fermi function under condition of 0 K. The lattice parameters calculated with the method described are close to the experiment results (see S1). The binding energy (54 Kcal/mol) of HgO is corresponding well with the values 53±8 Kcal/mol obtained from experiments[28]. Transition states are located with synchronous transit method that works best when reasonable structures of the reactants and products exist. Complete LST/QST calculations are conducted to confirm the predicted structures of the transition states[29].

3. Results and Discussion

In this section, the characteristics of minimum energy path identified for each elementary steps considered in this work (Figures 2 to 6) are discussed. Finally, Figure 7 compares the various pathways for mercury oxidation/chemical adsorption on $CuCo_2O_4$(110), based on the energetic of these steps.

3.1. The mercury oxidation/chemical adsorption on $CuCo_2O_4$ (110)

Shima[30] thought that Cu exists as Cu^{2+} in Co_3O_4 spinel crystal and the structure can be written as: $(Cu^{2+})[Co_2^{3+}]O_4$. Yogesh Sharma[31] synthesized nano $CuCo_2O_4$ with the structure of $Cu_xCo_{3-x}O_4$ ($x \geq 0.95$). Its cell length (i.e., a, 8.129 Å) is close to that of $Cu_{.95}Co_{2.05}O_4$, 8.133 Å. Although virgin $CuCo_2O_4$ crystal is difficult to be acquired, it can be used as a model on behalf of $Cu_xCo_{3-x}O_4$ for study of the mercury oxidation/chemical adsorption micro-mechanism [32-34]. As we can see, $CuCo_2O_4$ derived from spinel Co_3O_4 whose (110) crystal face was reported to be one of naturally exposed surfaces[35-37]. For comparison with Co_3O_4(110), in this paper, a periodic self-consistent DFT investigation of mercury oxidation/chemical adsorption on the surfaces of $CuCo_2O_4$(110) and different N-doped $CuCo_2O_4$(110) is performed.

The notation of atoms in the $CuCo_2O_4$(110) slab are shown in Fig. 1. Based on their locations and functions, oxygen atoms in $CuCo_2O_4$(110) slab are classified into three types: O_b, O_s, and O_w. O_b represents the oxygen atoms in the bulk of $CuCo_2O_4$(110) slab while O_s and O_w stand for those on the $CuCo_2O_4$(110) surface. O_w is bonded with one Cu^{2+} ion and one Co^{3+} ion while O_s is bonded to three Co^{3+} ions. O_w and O_s are in different crystal fields, thus possessing different reactivity.

The Hg atom around the O_s, O_w and $Co^{3+}{}_t$ (the subscript "t" in $Co^{3+}{}_t$ means the Co^{3+} on the top layer) on the $CuCo_2O_4$(110) surface can take different locations, but only one adsorption state (Hg_a), located on the top of $Co^{3+}{}_t$ is energetically favorable for physical adsorption.

The elementary steps associated with physical and chemical adsorption on the $CuCo_2O_4$(110) surface, and the relevant energy

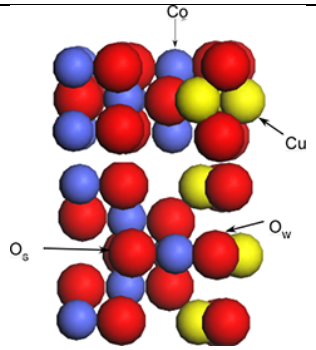

Fig. 1 The notation of atoms in $CuCo_2O_4$(110) slab and illustration of two orientations of $CuCo_2O_4$(110) slab. [Top: $CuCo_2O_4$(110) slab with (110) surface perpendicular to the paper; bottom: $CuCo_2O_4$(110) slab with (110) surface parallel to the paper].

profiles for possible reaction routes involving O_w and O_s have been studied. The results are presented in Fig. 2 (See S1 for the structure data).

The energy change in the first step or physical adsorption of gas-phase elementary mercury on $CuCo_2O_4$(110) is -0.25 eV and thus is exothermic. The calculated inter-atomic distances of Hg-$Co^{3+}{}_t$, Hg-O_w, and Hg-O_s are 2.75, 3.17 and 3.33 Å, respectively, which indicates no chemical bonds are formed among Hg-Co, Hg-O_s, and Hg-O_w. In other words, Hg atoms are only physically adsorbed on the surface of $CuCo_2O_4$ (110). The physical adsorption of Hg^o on the $CuCo_2O_4$(110) surface leads to the proximity of the Hg^0 atom to either O_w or O_s, and the formation of intermediates containing Hg-O-$Co^{3+}{}_t$ bond after passing the transition states of $(Hg\text{-}O_w)_{TS}$ or $(Hg\text{-}O_s)_{TS}$ with energy barriers of 0.85 or 1.83 eV, respectively. For the reverse reaction, the activation energy involving O_w is 0.28 eV and higher than that involving O_s (0.05 eV). Therefore, the intermediate M1 involving O_w is more stable than the intermediate involving O_s. Based on the activation energy values of forward and reverse reactions, the formation of M1 is a favorable mercury oxidation/chemical adsorption route. The bond length of Hg-O_w in $(Hg\text{-}O_w)_{TS}$ is 2.56 Å, which decreases to 2.47 Å when $(Hg\text{-}O_w)_{TS}$ change into M1.

For M1, there are three possible reaction pathways as shown in Fig. 3. The first pathway is the escape of HgO molecule from M1 to flue gas and leaves an oxygen vacancy (O_v) at O_w site, which is endothermic and needs 4 eV energy. The re-oxidation of O_v by O_2 in the flue gas leads to the healing of the surface and leaves an O radical. The second reaction pathway is the reaction between M1 and oxygen radical to produce HgO-slab and heal the O_v, which needs 1.71 eV activation energy and releases 1.75 eV energy as presented in Figure 3b. The third reaction pathway is that M1 overcomes 0.085 eV energy to form another intermediate M1′ (Fig. 2). M1′ can react with O_2 to form HgO-O-slab and release 1.05 eV energy. HgO-O-slab can further form HgO-slab and O-slab and the activation energy is 0.63 eV. Among them, HgO-slab is on behalf of the mercury oxide adsorption on $CuCo_2O_4$(110) surface and the adsorption energy is 3.13 eV.

3.2. The mercury oxidation/chemical adsorption on 1N doped $CuCo_2O_4$ (110)

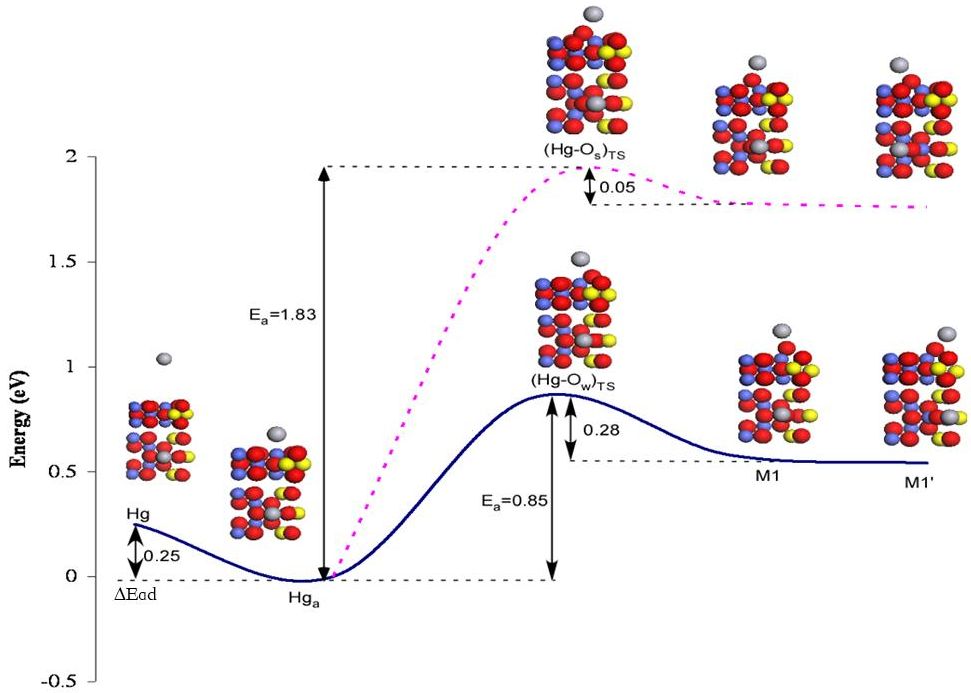

Fig. 2 Reaction pathways of Hg adsorption and oxidation on the virgin $CuCo_2O_4$ (110) surface. (Solid line: the reaction way through O_w; dot line: the reaction way through O_s).

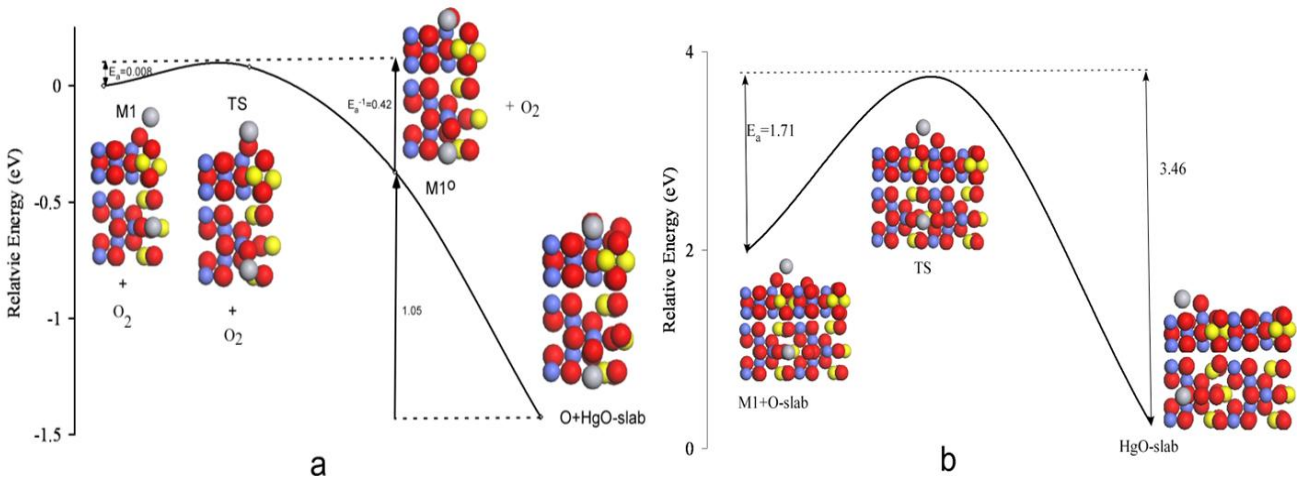

Fig. 3 Energy profile of the different reaction pathways between (a) M1 and O_2 and (b) M1 and O radical.

As presented in Fig. 1, there are three types of O atom (O_b, O_w, O_s) on $CuCo_2O_4$(110) slab, and all of them may be substituted by nitrogen atoms. When O_b is substituted by one N atom, there are two different reaction pathways involving O_s and O_w, respectively. Similarly, O_s or O_w can be substituted by N atom and there is one reaction pathway pertaining to O_w or O_s, respectively. The energy profiles of the four possible reaction pathways are shown in Fig. 4 (See S1 for the structure data). Among the structures resulting from different N substitutions, the one containing N_b has the lowest energy. This suggests that N atom prefers to replace the O atom in the bulk rather than on the surface, due to the fact that N is trivalent while O is divalent, and the bulk is better than the surface to satisfy the bonding requirement of N and reduce the formation of the dangling bonds on the surface. When O_b is substituted by Nitrogen atom, the transition state of the reaction pathway (solid line in Fig. 4) involving O_w has the lowest activation energy. Therefore, the mercury oxidation/chemical adsorption pathway involving O_w on the O_b substituted $CuCo_2O_4$(110) surface is favorable.

The first step of mercury oxidation/chemical adsorption on the surface of N-doped $CuCo_2O_4$(110) is the physical adsorption of mercury on slab (Hg_a), which releases 0.2 eV energy. The adsorption site is Co^{3+}_t and the length between Hg and Co^{3+}_t is 2.83 Å. The second step is similar to the oxidation/chemical adsorption of Hg on the surface of virgin $CuCo_2O_4$ (110) and the physically adsorbed Hg atom interacts with O_w to form M2

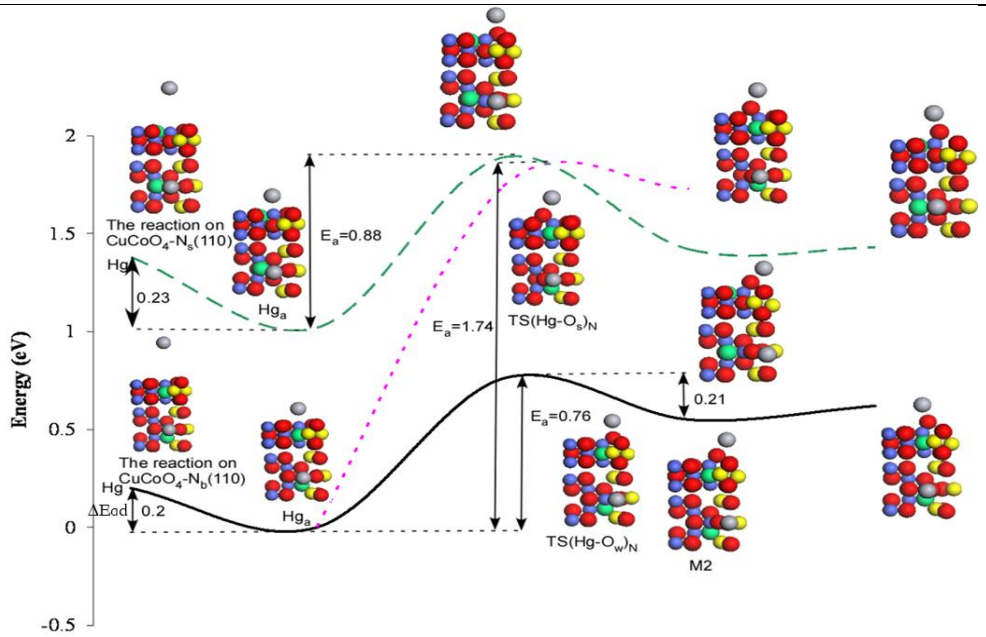

Fig. 4 Possible reaction pathways of Hg oxidation/chemical adsorption on different 1N doped $CuCo_2O_4$ (110) surfaces.

intermediate that contains Hg-O_w-Co^{3+}_t structure through overcoming an energy barrier of 0.76 eV.

As shown in the Fig. 4 (solid line), the transitional state and stable intermediate species of the most favorable reaction pathway are TS(Hg-O_w)$_N$ and M2, respectively. The distance between Hg and O_w changes from 3.21 to 2.59 Å, when Hg existence form changes from Hg_a to the transitional state, TS(Hg-O_w)$_N$. The distance continue decrease from 2.59 to 2.51 Å, when the Hg existence form changes from TS(Hg-O_w)$_N$ to M2. The structural parameter variation suggests a process of mercury adsorption going through physical adsorption to chemical adsorption on the N doped $CuCo_2O_4$ (110) surface. Compared with that (0.85 eV) on virgin $CuCo_2O_4$(110) surface, the activation energy (E_a) of mercury oxidation/chemical adsorption on 1N doped $CuCo_2O_4$(110) decreases to 0.76 eV.

3.3. The mercury oxidation/chemical adsorption on 2N doped $CuCo_2O_4$(110)

In this section, the mercury oxidation/chemical adsorption on two nitrogen doped $CuCo_2O_4$(110) surface is studied. When two O_b atoms on the virgin $CuCo_2O_4$(110) surface are substituted by the corresponding Nitrogen atoms, theoretically, two reaction pathways involving the O_w or O_s respectively should exist. However, the reaction pathway involving O_s cannot be found due to its low activity. For the same reason, when two N atoms substitute one O_b atom and one O_w atom, the reaction pathway involving the O_s does not exist. When two N atoms substitute one O_b and one O_s, the reaction pathway involving the O_w exists. The energy profiles of the two mercury oxidation/chemical adsorption pathways on 2N doped $CuCo_2O_4$(110) surface are shown in Fig. 5 (See S1 for the structure data).

Among different 2N doped $CuCo_2O_4$(110) slab, the $CuCoO_4$-N_{bb}(110), which represent the structure where two O_b in $CuCo_2O_4$(110) are substituted by Nitrogen, has the lowest energy, and is the most stable species. On the contrary, the structure of $CuCoO_4$-N_{bs}(110) possesses the highest energy. Although the reaction on the $CuCoO_4$-N_{bs}(110) surface requires the lowest activation energy (0.68 eV), it is not the most favorable reaction pathway due to its highest substitution energy. The doped structure must be thermally stable since it may decompose in a high temperature environment. Therefore, the pathway of mercury oxidation/chemical adsorption on $CuCoO_4$-N_{bb}(110) surface involving O_w is favorable under the situation of 2N doped $CuCo_2O_4$(110). The activation energy E_a of mercury oxidation/chemical adsorption on $CuCoO_4$-N_{bb}(110) surface (0.69 eV) is lower than that on 1N doped $CuCoO_4$-N_b(110) surface as obtained in the previous section (0.76 eV).

3.4. The mercury oxidation/chemical adsorption on 3N doped $CuCo_2O_4$(110)

For 3N doped $CuCo_2O_4$(110), theoretically, there are two mercury oxidation/ chemical adsorption pathways. When three N atoms substitute two O_b atoms and one O_w atom, the reaction pathway involves O_s. When three N atoms substitute two O_b and one O_s, the reaction pathway involves O_w. However, no reaction pathway exists when the mercury is adsorbed on 3N doped $CuCoO_4$-N_{bbw}(110) surface due to the low mercury oxidation/chemical adsorption ability of O_s. The energy profiles of mercury oxidation/chemical adsorption on 3N doped $CuCoO_4$-N_{bbs}(110) surface is given in Fig. 6. Although the mercury oxidation/chemical adsorption on 3N doped $CuCoO_4$-N_{bbs}(110) surface involving O_w atom possesses lower E_a (0.48 eV) and higher reverse reaction activation energy than that of the pathway on 2N doped $CuCo_2O_4$(110), it may not exist due to its thermodynamic instability. This is because structure $CuCoO_4$-N_{bbs}(110) has higher energy than $CuCoO_4$-N_{bbw}(110). Therefore, 3N doped $CuCo_2O_4$(110) is difficult to oxidize/chemical adsorb the mercury.

Based on the discussion of sections 3.1 - 3.4, the mercury oxidation/chemical adsorption network on $CuCo_2O_4$(110) and

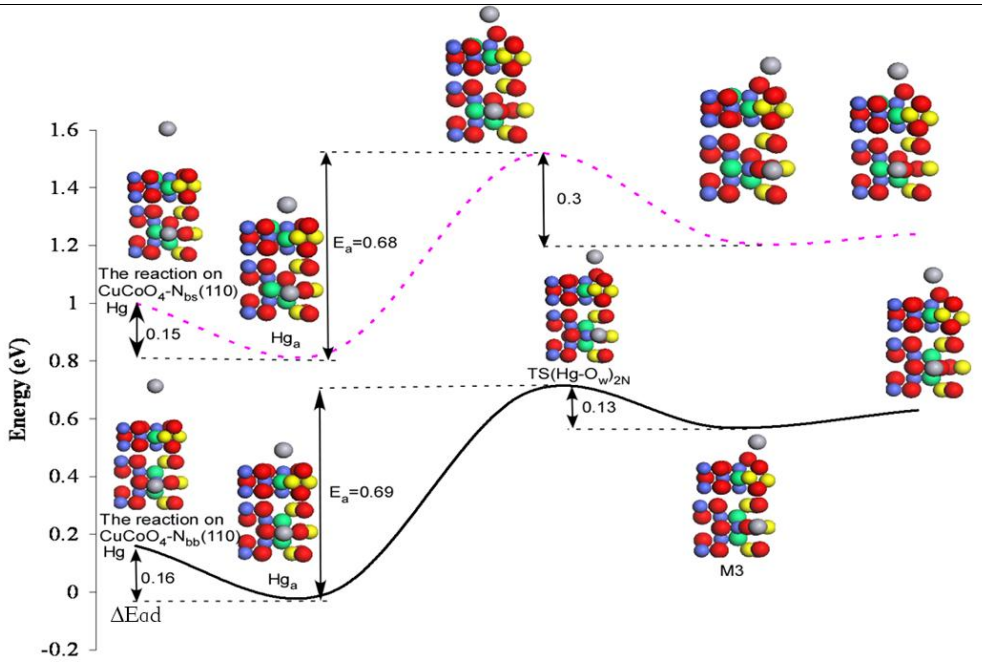

Fig. 5 Reaction pathways of Hg oxidation/chemical adsorption on different 2N doped $CuCo_2O_4$ (110) surfaces.

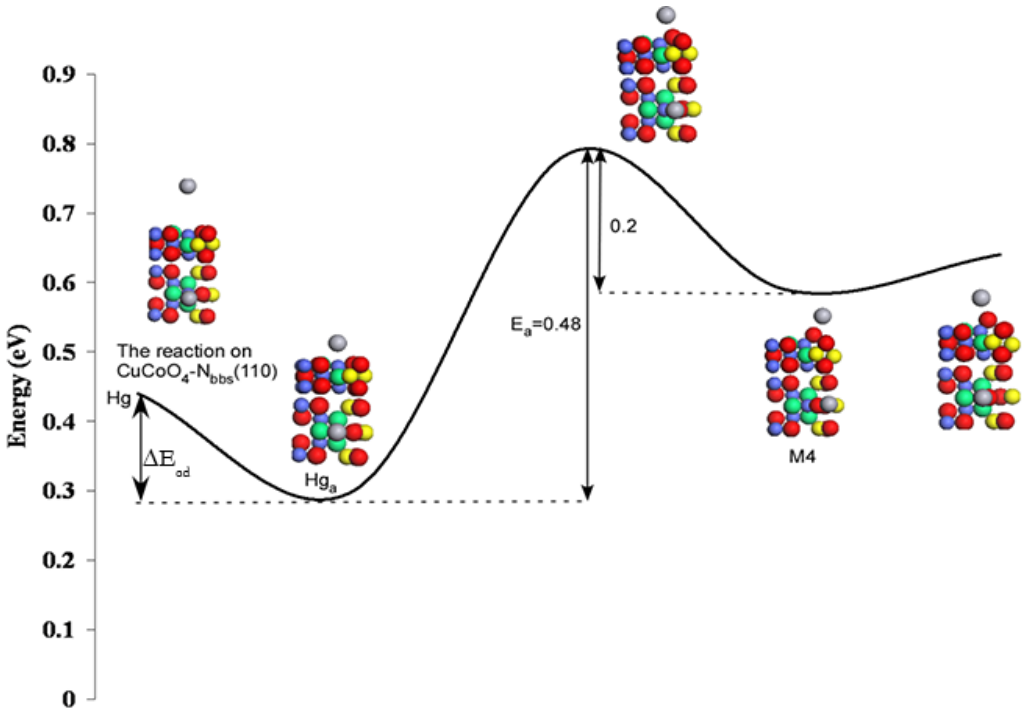

Fig. 6 Reaction pathways of Hg oxidation/chemical adsorption on different 3N doped $CuCo_2O_4$ (110) surface.

different N-doped $CuCo_2O_4$(110) surface is shown in Fig. 7. The factors affecting the mercury oxidation/chemical adsorption ability of different N doped $CuCo_2O_4$(110) include the activation energy of forward reaction (E_a) and reverse reaction (E_a^{-1}), the energy levels of N doped $CuCo_2O_4$(110) slab, and the number and location of N atoms doped on $CuCo_2O_4$(110). It should be emphasized that doped N atoms will replace O atoms located on the $CuCo_2O_4$(110) surface and thus reduce the number of the oxygen atoms that can oxidize the mercury. Therefore, there should be an optimal N-doping dosage to balance the effect of the O atoms decrease on the N-doped $CuCo_2O_4$ (110) surface and that of activation energy decrease due to N-doping. The experiment showed that, for N doped $CuCo_2O_4$, the optimal doping ration of N to Co is 30 mol%[20].

3.5 General comments on the mechanism of Hg^0 adsorption

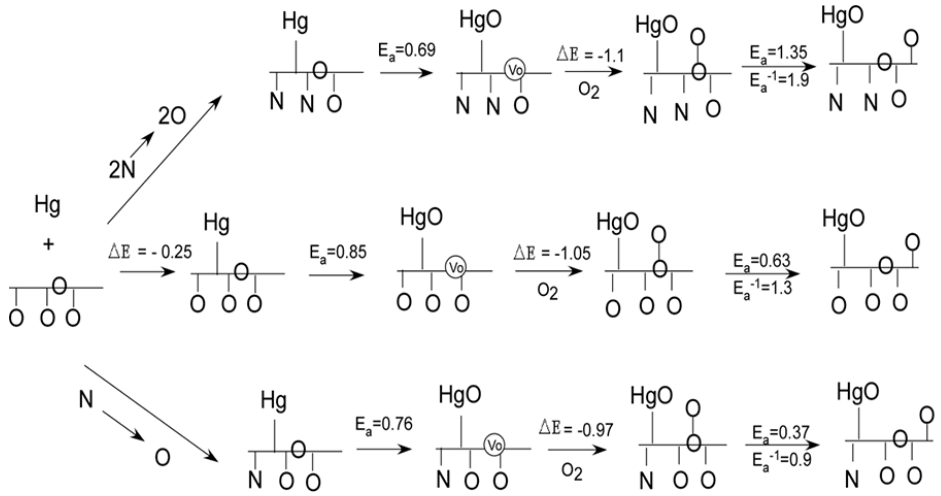

Fig. 7 Reaction network for mercury oxidation/chemical adsorption on $CuCo_2O_4$(110) and N-doped $CuCo_2O_4$(110) surface. The unit of thermochemistry and kinetic barrier data for the elementary steps is given in electron volts.

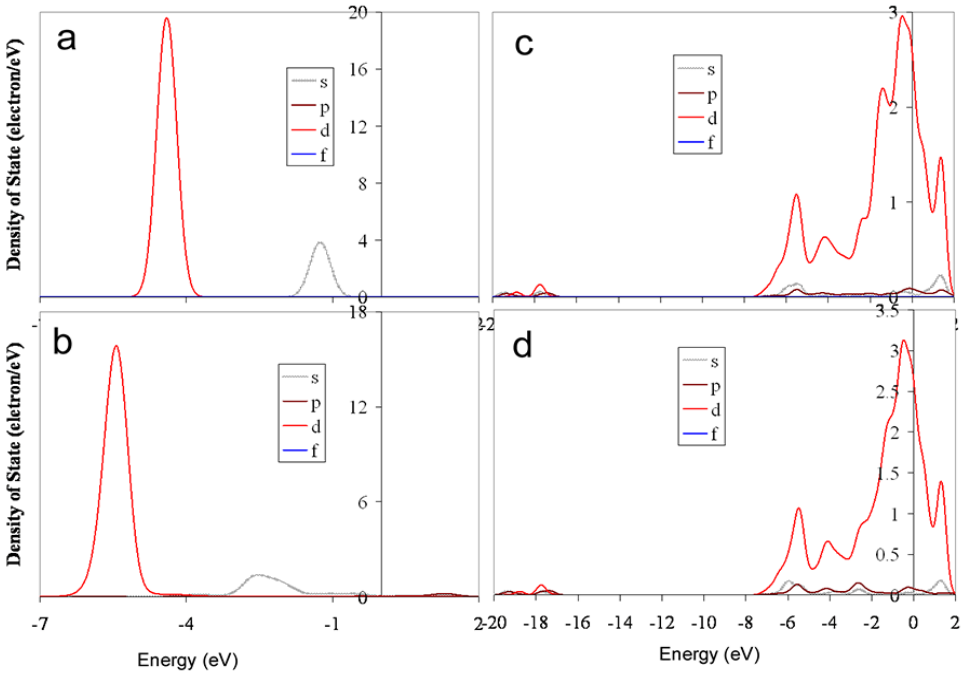

Fig. 8 The LDOS analysis of Co^{3+}_t and Hg before and after mercury physical adsorption on $CuCo_2O_4$(110) surface [a: Hg; b: Hg adsorbed on $CuCo_2O_4$(110); c: Co^{3+}_t; d: Co^{3+}_t with Hg adsorption].

on the different N-doped $CuCo_2O_4$ (110) surfaces

The parameters ΔE_{ad}, ΔE_{HgO}, E_a and E_a^{-1} of the favorable reaction pathways for virgin and N-doped $CuCo_2O_4$ (110) surfaces show some kinds of variation trends. Here, ΔE_{ad} is the mercury physical adsorption energy, ΔE_{HgO} is HgO adsorption energy; E_a is activation energy; and E_a^{-1} is the activation energy of reverse mercury oxidation/chemical adsorption. In addition to reducing the E_a, N-doping can also decrease the adsorption energies of mercury and mercuric oxide (S1 table2).

Experiments on mercury oxidation/chemical adsorption show that with a continuous increase of adsorption temperature from 373 to 623 K, the Hg^o removal ability of $CuCo_2O_4$ increases from 10 to 71.3%. Compared with virgin $CuCo_2O_4$, the Hg^0 oxidation ability of N doped $CuCo_2O_4$ reaches 91% at 623 K and is significantly higher, especially at low temperatures. The temperature independence of N doped $CuCo_2O_4$ indicates that N-doping greatly lowers the active energy of oxidation reaction. This is consistent with our DFT calculation results. When the temperature is above 623 K, the Hg^o removal abilities of $CuCo_2O_4$ and N doped $CuCo_2O_4$ decreases and those of N-doped $CuCo_2O_4$ decrease even faster than $CuCo_2O_4$[20]. The lower the E_a^{-1} is, the easier the reverse reaction of mercury oxidation will be.

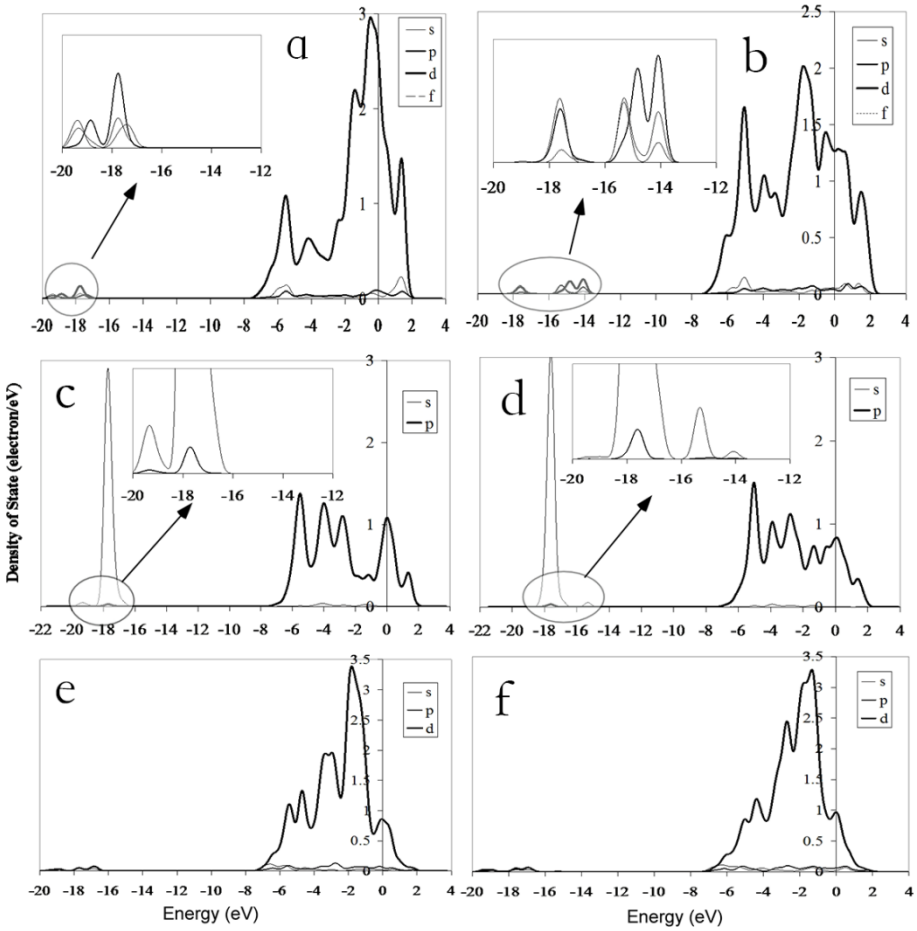

Fig. 9 The LDOS analysis of Co^{3+}_t, O_w, and Cu^{2+} in $CuCo_2O_4$ slab before and after 3N-doping. [a: Co^{3+}_t of $CuCo_2O_4$(110); b: Co^{3+}_t of $CuCoO_4$-N_{bbs}(110); c: O_w of $CuCo_2O_4$(110); d: O_w of $CuCoO_4$-N_{bbs}(110); e: Cu^{2+} of $CuCo_2O_4$(110); f: Cu^{2+} of $CuCoO_4$-N_{bbs}(110)].

As we can see, N-doping process decreases the E_a and E_a^{-1} at the same time. Furthermore, higher temperature would help the release of HgO from the sorbents' surface (i.e. the reactions of HgO-(slab-O_v) → HgO + (slab-O_v) and HgO-slab →HgO + slab). Due to these factors in forward and backward directions, there should be an optimal adsorption temperature to maximize the Hg^0 removal ability and capacity for $CuCo_2O_4$(110) and N-doped $CuCo_2O_4$(110). When the temperature increases over the optimal temperature in an environment of lower mercury partial pressure, the chemically adsorbed mercury can be released into gas phase and spent $CuCo_2O_4$ can be regenerated[20].

Natural Bond Orbital (NBO) analysis using Gaussian 03 shows that when mercury adsorbs on $CuCo_2O_4$(110) surface, its 6s(α) orbital hybrids with Co^{3+} orbital forming BD(1)Co^{3+}_t-Hg and BD*(1)Co^{3+}_t-Hg (BD represents bonding orbital and BD* represents anti-bonding orbital) which distribute the electron over the system (S1 table3 and table 4). When O_b is substituted by N, the interaction between LP(6s)Hg (LP represents lone pair) and BD(1)*Co^{3+}_t-O_b will be replaced by the interaction between LP(6s)Hg and BD(1)*Co^{3+}_t-N_b. The latter has less second order perturbation stabilization energies. Therefore, N-doped sorbents will have lower physical Hg^0 adsorption energies.

Local Density of State (LDOS) analyses show the contribution of an atom's electronic states to the electronic hybridization in the system and thus the qualitative reflection in the energy spectrum. Fig. 8 shows that when mercury is not adsorbed by $CuCo_2O_4$(110) slab, the energy band of its 6s orbital is located at -1.3 eV and that of 5d is located at -4.5 eV. When mercury is physically adsorbed by $CuCo_2O_4$(110), its 6s and 5d energy bands shift to -2.7 and -5.6 eV, respectively. The energy bands of Co^{3+}_t are located between -7.5 and 2 eV. Since the size of Co^{3+} is much smaller than that of Hg^0 atom and Co^{3+} located on the surface of slab, its electronic orbitals are hard to be polarized. Thus, the energy bands of Co^{3+}_t do not have apparent changes before and after Hg^0 adsorption.

In order to understand the effect of N-doping on $CuCo_2O_4$(110) slab, the LDOS analyses of Hg adsorption on virgin $CuCo_2O_4$(110) and 3N doped $CuCo_2O_4$(110) surfaces are shown in Fig. 9. N doping will affect the orbit hybrid status of Co^{3+}_t in the slab. From Figure 9, we can see that the replacement of O_b and O_s by N will introduce a new energy band for Co^{3+}_t between -13 and -16 eV, but reduces the peak height of the energy band between -18 ~ -20 eV. The electronic status change of Co^{3+}_t can affect the electronic status of O_w bonded to Co^{3+}_t. We can see that the small energy band of O_w at -19.5 eV disappears, and a new small energy band appears at -15 eV. However, the energy band of Cu^{2+} connecting to O_w does not shift (keeps between -17 and -20 eV). Therefore, the bond strength between O_w and Cu^{2+}

is decreased and O_w of 3N doped $CuCo_2O_4$(110) becomes more active than that of $CuCo_2O_4$(110).

4. Conclusions

The mercury oxidation/chemical adsorption on virgin $CuCo_2O_4$(110) and different N doped $CuCo_2O_4$(110) surfaces are studied. The detailed energy profiles of the possible reaction pathways are discussed. Based on their activation energy, the energy levels of N doped $CuCo_2O_4$(110) slab, the stability of physical or chemical adsorption intermediates, the favorite reaction pathways are selected and thus the detailed mechanisms are provided. By analyzing the calculation results, we found that the O_w is the most active site on the surface of $CuCo_2O_4$(110) and the N-doping can increase the activity of O_w through increasing the LDOS at higher energy and deactivate that of O_s at the same time. Due to O_w's high activity, the activation energy of mercury oxidation/chemical adsorption decreases from 0.85 eV (virgin $CuCo_2O_4$(110)) to 0.69 eV (2N doped $CuCo_2O_4$(110)). The LDOS analyses demonstrate that the doped N atom decrease the bond strength between O_w and Cu which activate O_w further.

Notes and references

[a] *School of Environmental Sciences and Resource, Inner Mongolia University, No.235 West College Road, Hohhot, Inner Mongolia 010021, P.R.China. Tel:+08613029512441; E-mail: meizhijian@hotmail.com*
[b] *Chemical & Petroleum Engineering Department, University of Wyoming, Laramie, WY 82071, USA*
[c] *School of Civil and Environmental Engineering, Georgia Institute of Technology, Atlanta, GA 30332, USA*
[d] *School of Environmental Science and Engineering, Shanghai Jiao Tong University, 800 Dong Chuan Road, Shanghai 200240, China*

† Electronic Supplementary Information (ESI) available: [S1: the structrue data of some important intermediates]. See DOI: 10.1039/b000000x/

1. E. Alizadeh-Gheshlaghi, B. Shaabani, A. Khodayari, Y. Azizian-Kalandaragh and R. Rahimi, *Powder Technology*, 2012, **217**, 330-339.
2. J. Zhu and Q. Gao, *Microporous and Mesoporous Materials*, 2009, **124**, 144-152.
3. K. De, Mathieu, Poirier, C. Simon, Marsan and Benoit, *Cu[x]Co[3-][x]O[4] used as bifunctional electrocatalyst. II. Electrochemical characterization for the oxygen reduction reaction*, Electrochemical Society, Pennington, NJ, ETATS-UNIS, 2007.
4. A. La Rosa-Toro, R. Berenguer, C. Quijada, F. Montilla, E. Morallón and J. L. Vázquez, *The Journal of Physical Chemistry B*, 2006, **110**, 24021-24029.
5. N. Fradette and B. Marsan, *Journal of The Electrochemical Society*, 1998, **145**, 2320-2327.
6. R. Bonchev, T. Zheleva and S. C. Sevov, *Chemistry of Materials*, 1990, **2**, 93-95.
7. J. Wang, P. A. Chernavskii, Y. Wang and A. Y. Khodakov, *Fuel*, 2013, **103**, 1111-1122.
8. S. Varghese, M. G. Cutrufello, E. Rombi, C. Cannas, R. Monaci and I. Ferino, *Applied Catalysis A: General*, 2012, **443-444**, 161-170.
9. Z. Mei, Z. Shen, Q. Zhao, T. Yuan, Y. Zhang, F. Xiang and W. Wang, *Chemosphere*, 2008, **70**, 1399-1404.
10. Y. Sharma, N. Sharma, G. V. S. Rao and B. V. R. Chowdari, *Journal of Power Sources*, 2007, **173**, 495-501.
11. Y. Sharma, N. Sharma, G. V. Subba Rao and B. V. R. Chowdari, *Advanced Functional Materials*, 2007, **17**, 2855-2861.
12. Baird, T, Campbell, C. K, Holliman, J. P, Hoyle, W. R, Huxam, M, Stirling, D, Williams, P. B, Morris and M, *Cobalt-zinc oxide absorbents for low temperature gas desulfurisation*, Royal Society of Chemistry, Cambridge, ROYAUME-UNI, 1999.
13. J. F. Marco, J. R. Gancedo, M. Gracia, J. L. Gautier, Rı, amp, x, E. os and F. J. Berry, *Journal of Solid State Chemistry*, 2000, **153**, 74-81.
14. P. Boldrin, A. K. Hebb, A. A. Chaudhry, L. Otley, B. Thiebaut, P. Bishop and J. A. Darr, *Industrial & Engineering Chemistry Research*, 2007, **46**, 4830-4838.
15. G. Fortunato, H. R. Oswald and A. Reller, *Journal of Materials Chemistry*, 2001, **11**, 905-911.
16. W. Wei, W. Chen and D. G. Ivey, *Chemistry of Materials*, 2008, **20**, 1941-1947.
17. R. Asahi, T. Morikawa and T. Ohwaki, *Science*, 2001, **293**, 269-271.
18. H. X. Dai, C. F. Ng and C. T. Au, *Journal of Catalysis*, 2001, **197**, 251-266.
19. H. X. Dai, C. F. Ng and C. T. Au, *Journal of Catalysis*, 2000, **189**, 52-62.
20. Z. Mei, Z. Shen, Z. Mei, Y. Zhang, F. Xiang, J. Chen and W. Wang, *Applied Catalysis B: Environmental*, 2008, **78**, 112-119.
21. C. Doornkamp and V. Ponec, *Journal of Molecular Catalysis A: Chemical*, 2000, **162**, 19-32.
22. M. Altarawneh and S. A. Saraireh, *Physical Chemistry Chemical Physics*, 2014, DOI: 10.1039/C4CP00220B.
23. M. Rubes, J. Kysilka, P. Nachtigall and O. Bludsky, *Physical Chemistry Chemical Physics*, 2010, **12**, 6438-6444.
24. M. Al-Shakran, G. Beltramo and M. Giesen, *Physical Chemistry Chemical Physics*, 2014, DOI: 10.1039/C4CP00448E.
25. C. E. Szakacs, M. Lefevre, U. I. Kramm, J.-P. Dodelet and F. Vidal, *Physical Chemistry Chemical Physics*, 2014, DOI: 10.1039/C3CP55331K.
26. J. P. Perdew, K. Burke and M. Ernzerhof, *Physical Review Letters*, 1996, **77**, 3865-3868.
27. P. Broqvist, I. Panas and H. Persson, *Journal Catalysis*, 2002, **210**, 198-206.
28. M. Filatov and D. Cremer, *Chemphyschem : a European journal of chemical physics and physical chemistry*, 2004, **5**, 1547-1557.
29. X.-L. Xu, Z.-H. Chen, Y. Li, W.-K. Chen and J.-Q. Li, *Surface Science*, 2009, **603**, 653-658.
30. M. Shimada, F. Kanamaru, M. Koizumi and N. Yamamoto, *Materials Research Bulletin*, 1975, **10**, 733-736.
31. Y. Sharma, N. Sharma, G. V. S. Rao and B. V. R. Chowdari, *Journal of Power Sources*, 2007, **173**, 495-501.
32. M. De Koninck, S.-C. Poirier and B. Marsan, *Journal of the Electrochemical Society*, 2007, **154**, A381-A388.
33. A. La Rosa-Toro, R. Berenguer, C. Quijada, F. Montilla, E. Morallon and J. L. Vazquez, *Journal of Physical Chemistry B*, 2006, **110**, 24021-24029.
34. D. Panaiotov, V. Matyshak, A. Sklyarov, A. Vlasenko and D. Mekhandzhiev, *Applied Catalysis*, 1986, **24**, 37-51.
35. X. L. Xu and J. Q. Li, *Surface Science*, 2011, **605**, 1962-1967.
36. S. C. Petitto and M. A. Langell, *Surface Science*, 2005, **599**, 27-40.
37. E. M. Malone, S. C. Petitto and M. A. Langell, *Solid State Communications*, 2004, **130**, 571-575.